CAAI Transactions on Intelligence Technology

WILEY

The Institution of Engineering and Technology

ORIGINAL RESEARCH OPEN ACCESS

Convergent Interval Confirmation for Three-Step Discrete Specific Zeroing Neural Dynamics Illustrated With Repetitive Motion Planning of Redundant Manipulators

Ying Kong[1] | Shaoyuan Sun[1] | Yunliang Jiang[2,3,4] | Lin Wei[5]

[1]School of Computer Science and Technology, Zhejiang University of Science and Technology, Hangzhou, China | [2]Zhejiang Key Laboratory of Intelligent Education Technology and Application, Zhejiang Normal University, Jinhua, China | [3]School of Computer Science and Technology, Zhejiang Normal University, Jinhua, China | [4]School of Information Engineering, Huzhou University, Huzhou, China | [5]School of Electrical and Electronic Engineering, Nanyang Technological University, Singapore, Singapore

Correspondence: Yunliang Jiang (jyl@zjhu.edu.cn)

Received: 3 July 2025 | **Revised:** 15 November 2025 | **Accepted:** 10 December 2025

Keywords: convergent error constant | redundant manipulator | repetitive motion planning (RMP) | three-step discrete specific zeroing neural dynamics (TS-DSZND)

ABSTRACT

Repetitive motion planning (RMP) for redundant manipulators with high convergent precision becomes an intense research topic due to its more degrees of freedom. In this paper, a specific zeroing neural dynamics (SZND) model for the RMP is first set up via zeroing neurodynamics. After that, a general linear three-step rule is presented and applied to discretise the SZND model. Then, we obtain a three-step discrete SZND (TS-DSZND) model for repetitive kinematics. It is necessary to point out that the stepsize in TS-DSZND algorithm is intimated to the stability of the proposed TS-DSZND. By utilizing linear transformation and the Jury stability criterion, the optimal stepsize interval of the TS-DSZND is obtained by a theorem. Furthermore, the truncation error constant, which tends to be neglected with most of the ZeaD-typed discretisation formulas for the RMP of redundant manipulators, is analysed and exhibits the impact for the convergent accuracy compared with the corresponding three-step rules. Besides, simulative illustrations on various redundant manipulators show the superiority and feasibility of the proposed TS-DSZND as well as the effective stepsize domain. Finally, a physical experiment on a real UR5 robotic arm for fulfiling a flower-shaped path validates the satisfying performance of the TS-DSZND model.

1 | Introduction

Redundant manipulators have been playing an increasing important role recently. In many engineering applications, redundant manipulators have been widely applied in many areas of medical engineering [1, 2], motion planning [3, 4] and cruise control [5, 6] because manipulators do not get tired and can release humans from complex, dangerous and repeatable works.

With the development of science information technologies, discussions about the kinematic planning of redundant manipulators have been emphasized by many researchers. Redundant manipulators have more degrees of freedom than the work required, which induces its flexibility in many engineering fields. Given a trajectory task of the end effector, there may exist a variety of algorithms for the kinematic manipulators. We can choose from the methodologies by considering extra requirements, for example, harmonic noises suspending [7], reinforcement learning [8] and optimal manipulability task [9, 10]. Researchers realized the noises' avoidance for redundant manipulators, which is verified by the manipulator PUMA560. For example, in [7], it proposed a deformed primal-dual network (PDN) for regulating the trajectories of manipulators

This is an open access article under the terms of the Creative Commons Attribution License, which permits use, distribution and reproduction in any medium, provided the original work is properly cited.

© 2026 The Author(s). *CAAI Transactions on Intelligence Technology* published by John Wiley & Sons Ltd on behalf of The Institution of Engineering and Technology and Chongqing University of Technology.

regardless of the harmonic noises. This kind of PDN solvers was established to plan the joint position trajectories through minimizing the energy of kinematic joints. In [11], cooperative behaviours of multiple manipulators with a distributed neural network were presented from the game-illustrative perspective. In [12], Li *et* al. discussed the calibration technology and methodologies of industrial noises. However, these continuous algorithms are greatly dependent on the precise Jacobian matrix of the kinematic equation. In some situations, the configuration of the Jacobian matrix is unknown or is not accurate especially in some discretised neurodynamics [13, 14]. For instance, in [15], an adaptive neural model for computing an unpredictive Jacobian matrix was proposed and can achieve high-precision trajectory theoretically. Therefore, how to obtain high-precision trajectory with an accurate discrete formula for the Jacobian matrix is meaningful.

In recent years, neural network–based models are fast developed for solving the multifarious engineering problems, such as face identification [9], auto pilot [16] and kinematic calibration [17]. As a special kind of the recurrent neural network (RNN), zeroing neural network (ZNN) exhibits the strong ability for getting the solution of the time-variant problems [18]. Meanwhile, many neurodynamics based on the ZNN design formula have sprung up, which are sorted as zeroing neural dynamics (ZND). The motion process of a redundant manipulator is thought as a dynamic system varying with time actually. The particular 'ZND' formula is widely applied to optimize the motion trajectories of redundant manipulators. For making up the gap between real-world environment and ideal simulated platform, a coevolutionary neural network was proposed with swarm optimization for nonconvex optimization problems obtaining fast convergence [19]. Theoretical discussions on different kinematic plannings of redundant manipulators show the effectiveness of the continuous ZND model. However, continuous dynamical models are not easy for the digital computer operation due to the discretisation of digital information in real application. Therefore, for better understanding, the corresponding discrete model [20] is developed for the synchronized kinematic control of manipulators in real workspaces.

Following the above content and inspiration, discrete ZND (DZND) formulae with different discrete ZeaD (Zhang et al. discretisation) steps were focused for kinematic motion of robotic manipulators in [8, 21, 22]. However, the truncation error constant $C_pO(\tau^p)$ that is closely related to the convergent precision tends to be neglected [21]. Furthermore, the effective stepsize domains for the dynamic stability is few to be considered [23, 24]. Actually, if the time step τ is set larger, the truncation error constant C_p can greatly influence the truncation order $O(\tau^p)$. To improve the convergent precision and confirm the stepsize domain of stability, a three-step ZeaD formula as well as a specific ZND (SZND) model are integrated for kinematic repetitive planning of redundant manipulators in this paper. It is necessary to note that the traditional ZND is focusing on the joint velocities as optimization variables, whereas the specific ZND model utilizes joint positions as target variables, which leads to different derivative informations in a discretisation formula. Furthermore, the corresponding TS-DSZND model with a truncation error constant C_p is analysed in detail here. The advantage of the TS-DSZND model is proved not only in the theorem but also with abundant experiments. The relative comparisons among the existed three-step ZeaD-typed neural models and the proposed TS-DSZND are listed in Table 1. The main motivations can be summarized as follows: First, the integral-type unit of the RNN model is usually hard to be discretised for improper variable regulations. Second, although some continuous models are discretised in the end, the stability domain of the discretisation rule is not guaranteed, for example, a kind of DZND for motion planning of robotics [27] or adaptive projection RNN in [28]. Third, discretised models are convergent, consistent and stable, and the convergent accuracy can be enhanced to some extent. The position calculation of each joint is not derived from the simulation module but is simplified utilizing the three-step ZeaD formula as well although literatures [25] were concerned about trajectory planning with an approximate estimation of each joint position, which is obtained from the derivative information of joint velocity directly. The unified discretisation law for joint angles may appear rigorous and demanding for a dynamic optimization system with exquisite requirements. For generalization, in this paper, the initial position of each joint is supposed at an arbitrary position. However, the initial position of the end effector was strictly demanded at the desired position [26]. The corresponding SZND model and the corresponding three-step ZeaD rule are unified, and the strict stability and the larger stepsize domain are ultimately compared with the existing DZND methodologies.

The structure of this paper can be divided into the following six parts. In Section 2, the trajectory planning problem and the SZND model is presented. Theoretical analyses of the TS-DSZND model are provided in Section 3. In Section 4, plenty of example simulations are conducted to verify the theoretical results. Physical experiments on UR5 manipulators are executed for real application in Section 5. The conclusion of the paper is in Section 6. The highlights are summarized below as follows:

1. A general three-step discrete SZND (TS-DSZND) model with order $O(\tau^3)$ is presented and discussed for the RMP of redundant manipulators, which is inclined to be realized in computer hardware operation. Furthermore, the convergent truncation error constant is also considered, as it influences the convergence accuracy compared with the corresponding three-step discrete schemes.
2. The effective stepsize interval for the proposed TS-DSZND model is confirmed, which fully guarantees the stability of the TS-DSZND model.
3. The stability and convergent precision characteristics of the TS-DSZND are verified in theoretical analyses and demonstrated by various experimental results of redundant manipulators.
4. A physical experiment on the UR5 robot arm is carried out to attest the capability and application of the TS-DSZND model in an applied circumstance.

TABLE 1 | Comparisons between the existing three-step ZeaD-typed discretisations and the TS-DSZND.

	Discretisation formula	Error constant	Stability domain	Truncation error
This paper	YES	YES	COMPLETE	$O(g^3)$
Paper [15]	YES	NO	INCOMPLETE	$O(g^3)$
Paper [25]	YES	NO	INCOMPLETE	$O(g^4)$
Paper [26]	YES	NO	INCOMPLETE	$O(g^3)$

2 | Problem Formulation and a Specific ZND Model

In this part, kinematic equations about redundant manipulators and manipulation optimizations are presented. The continuous ZND model with an approximate Jacobian matrix is studied [28].

2.1 | Problem Formulation

For the redundant manipulator, the forward kinematics in Cartesian space can be expressed as

$$f(\theta_{k+1}) = \boldsymbol{r}_{k+1} \tag{1}$$

where $f(\cdot)$ is the nonlinear forward kinematics mapping function for the given manipulator. $\theta_{k+1} = \theta(t_{k+1}) \in \mathbb{R}^n$ and $\boldsymbol{r}_{k+1} = \boldsymbol{r}(t_{k+1}) \in \mathbb{R}^m$ of the end effector are measured from the smoothly joint angle $\theta(t) \in \mathbb{R}^n$ at time instant t_{k+1}. Taking the time derivative of the aforementioned kinematic Equation (1), we obtain

$$J(\theta_{k+1})\dot{\theta}_{k+1} = \dot{\boldsymbol{r}}_{k+1} \tag{2}$$

where $J(\theta_{k+1}) = \partial f(\theta)/\partial\theta \in \mathbb{R}^{m\times n}$ is the Jacobian matrix at time instant t_{k+1}.

The discrete repetitive motion planning (DRMP) of redundant manipulators is formulated during $[t_k, t_{k+1}) \subseteq [t_0, t_f] \subseteq [0, +\infty)$

$$\begin{aligned} \min_{\dot{\theta}\in\boldsymbol{R}^n} \quad & \frac{1}{2}\dot{\theta}_{k+1}^{\mathrm{T}}\dot{\theta}_{k+1} + \boldsymbol{c}^{\mathrm{T}}\dot{\theta}_{k+1} \\ \text{s.t.} \quad & J(\theta_{k+1})\dot{\theta}_{k+1} = \dot{\boldsymbol{r}}_{k+1} \end{aligned} \tag{3}$$

where $\boldsymbol{c} = \gamma(\theta_{k+1} - \theta_0)$ with $\gamma \in \mathbb{R}^+$ is to minimize the distance of joint displacement. t_0 and t_f represent the initial instant and final time instants, respectively. Besides, $J(\theta_{k+1}) = J(\theta(t_{k+1})) \in \mathbb{R}^{m\times n}$, $\theta_{k+1} = \theta(t_{k+1}) \in \mathbb{R}^n$ and $\dot{\boldsymbol{r}}_{k+1} = \dot{\boldsymbol{r}}(t_{k+1}) \in \mathbb{R}^m$ are generated from the smoothly time-dependent signals $\theta(t) \in \mathbb{R}^n$ and $\dot{\boldsymbol{r}}_{k+1}(t) \in \mathbb{R}^m$ by sampling at time instant t_{k+1}.

2.2 | SZND Model

To realize the discrete repetitive trajectory tracking problem of redundant manipulators, the corresponding continuous-time repetitive motion programme (CTRMP) containing the relative joint information is developed

$$\begin{aligned} \min_{\dot{\theta}\in\boldsymbol{R}^n} \quad & \frac{1}{2}\dot{\theta}^{\mathrm{T}}\dot{\theta} + \boldsymbol{c}^{\mathrm{T}}\dot{\theta} \\ \text{s.t.} \quad & J(\theta)\dot{\theta} = \dot{\boldsymbol{r}} \end{aligned} \tag{4}$$

where $\dot{\theta} = \dot{\theta}(t)$, $\theta = \theta(t)$ and $\dot{\boldsymbol{r}} = \dot{\boldsymbol{r}}(t)$. Using the Lagrange multiplier method, we can obtain a Lagrange function

$$L\left(\dot{\theta}, \boldsymbol{l}, t\right) = \dot{\theta}^{\mathrm{T}}\dot{\theta}/2 + \boldsymbol{c}^{\mathrm{T}}\dot{\theta} + \boldsymbol{l}^{\mathrm{T}}\left(J(\theta)\dot{\theta} - \dot{\boldsymbol{r}}\right)$$

where $\boldsymbol{l} = \boldsymbol{l}(t) \in \mathbb{R}^m$ shows the Lagrange-multiplier. By taking partial derivatives, the following two equations, which is consistent with CTRMP (4) is obtained:

$$\begin{aligned} \frac{\partial L\left(\dot{\theta}, \boldsymbol{l}, t\right)}{\partial\dot{\theta}} &= \dot{\theta} + \boldsymbol{c} + J(\theta)^{\mathrm{T}}\boldsymbol{l} = 0, \\ \frac{\partial L\left(\dot{\theta}, \boldsymbol{l}, t\right)}{\partial\boldsymbol{l}} &= J(\theta)\dot{\theta} - \dot{\boldsymbol{r}} = 0. \end{aligned}$$

According to the ZND model in [17], an error function is defined as

$$\boldsymbol{e}\left(\theta, \dot{\theta}, \boldsymbol{l}, t\right) = \begin{bmatrix} I & J(\theta)^{\mathrm{T}} \\ J(\theta) & 0 \end{bmatrix}\begin{bmatrix} \dot{\theta} \\ \boldsymbol{l} \end{bmatrix} + \begin{bmatrix} \boldsymbol{c} \\ -\dot{\boldsymbol{r}} \end{bmatrix} \tag{5}$$

where $I \in \mathbb{R}^{n\times n}$ is the identity matrix. According to the ZND formula, we get

$$\dot{\boldsymbol{e}}\left(\theta, \dot{\theta}, \boldsymbol{l}, t\right) = -\lambda\boldsymbol{e}\left(\theta, \dot{\theta}, \boldsymbol{l}, t\right) \tag{6}$$

where $\lambda \in \mathbb{R}^+$ is a scaling parameter regarding the convergent rate of the ZND formula. Assuming that error function $\boldsymbol{e}\left(\theta, \dot{\theta}, \boldsymbol{l}, t\right)$ is differentiable, its derivative with respect to time can then be found by the following chain rule:

$$\dot{\boldsymbol{e}}\left(\theta, \dot{\theta}, \boldsymbol{l}, t\right) = \frac{\partial\boldsymbol{e}}{\partial\theta}\dot{\theta} + \frac{\partial\boldsymbol{e}}{\partial\dot{\theta}}\dot{\theta} + \frac{\partial\boldsymbol{e}}{\partial\boldsymbol{l}}\dot{\boldsymbol{l}} + \frac{\partial\boldsymbol{e}}{\partial t}. \tag{7}$$

Theorem 1. *With $\theta \in \mathbb{R}^n$ denoting the joints state of the CTRMP (4), the Jacobian matrix $J(\theta) \in \mathbb{R}^{m\times n}$ actually represents*

a function of the joint angle θ. Assuming $J(\theta)$ is differentiable, we have the following results.

$$\frac{\partial\left(J(\theta)\dot{\theta}\right)}{\partial\theta} = H_1(\theta)\left(\dot{\theta}\otimes I\right),$$
$$\frac{\partial\left(J^{\mathrm{T}}(\theta)\boldsymbol{l}\right)}{\partial\theta} = H_2(\theta)(\boldsymbol{l}\otimes I)$$

where $\otimes$ represents Kronecker product. $H_1(\theta) = \partial J(\theta)/\partial\theta \in \mathbb{R}^{m\times nn}$ and $H_2(\theta) = \partial J^{\mathrm{T}}(\theta)/\partial\theta \in \mathbb{R}^{n\times mn}$ can be expressed as

$$H_1(\theta) = \begin{bmatrix} \frac{\partial j_{11}}{\partial\theta} & \frac{\partial j_{12}}{\partial\theta} & \cdots & \frac{\partial j_{1n}}{\partial\theta} \\ \frac{\partial j_{21}}{\partial\theta} & \frac{\partial j_{22}}{\partial\theta} & \cdots & \frac{\partial j_{2n}}{\partial\theta} \\ \cdots & \cdots & \cdots & \cdots \\ \frac{\partial j_{m1}}{\partial\theta} & \frac{\partial j_{m2}}{\partial\theta} & \cdots & \frac{\partial j_{mn}}{\partial\theta} \end{bmatrix},$$

$$H_2(\theta) = \begin{bmatrix} \frac{\partial j_{11}}{\partial\theta} & \frac{\partial j_{21}}{\partial\theta} & \cdots & \frac{\partial j_{m1}}{\partial\theta} \\ \frac{\partial j_{12}}{\partial\theta} & \frac{\partial j_{22}}{\partial\theta} & \cdots & \frac{\partial j_{m2}}{\partial\theta} \\ \cdots & \cdots & \cdots & \cdots \\ \frac{\partial j_{1n}}{\partial\theta} & \frac{\partial j_{2n}}{\partial\theta} & \cdots & \frac{\partial j_{mn}}{\partial\theta} \end{bmatrix}.$$

Proof: Because $\partial\left(J(\theta)\dot{\theta}\right)/\partial\theta$ is a partial derivative of θ, $\dot{\theta}$ should be considered as a constant, which can be rewritten as follows:

$$\begin{aligned} \frac{\partial\left(J(\theta)\dot{\theta}\right)}{\partial\theta} &= \begin{bmatrix} \sum_{p=1}^{n}\frac{\partial j_{1p}}{\partial\theta_1}\dot{\theta}_p, & \cdots & ,\sum_{p=1}^{n}\frac{\partial j_{1p}}{\partial\theta_n}\dot{\theta}_p \\ \cdots & \cdots & \cdots \\ \sum_{p=1}^{n}\frac{\partial j_{mp}}{\partial\theta_1}\dot{\theta}_p, & \cdots & ,\sum_{p=1}^{n}\frac{\partial j_{mp}}{\partial\theta_n}\dot{\theta}_p \end{bmatrix} \\ &= \begin{bmatrix} \frac{\partial j_{11}}{\partial\theta} & \frac{\partial j_{12}}{\partial\theta} & \cdots & \frac{\partial j_{1n}}{\partial\theta} \\ \frac{\partial j_{21}}{\partial\theta} & \frac{\partial j_{22}}{\partial\theta} & \cdots & \frac{\partial j_{2n}}{\partial\theta} \\ \cdots & \cdots & \cdots & \cdots \\ \frac{\partial j_{m1}}{\partial\theta} & \frac{\partial j_{m2}}{\partial\theta} & \cdots & \frac{\partial j_{mn}}{\partial\theta} \end{bmatrix} \begin{bmatrix} \dot{\theta}_1 I \\ \dot{\theta}_2 I \\ \cdots \\ \dot{\theta}_n I \end{bmatrix} \\ &= H_1(\theta)\left(\dot{\theta}\otimes I\right). \end{aligned}$$

The process of the derivation of $\partial\left(J^{\mathrm{T}}(\theta)\boldsymbol{l}\right)/\partial\theta = H_2(\theta)(\boldsymbol{l}\otimes I)$ is similar to $\partial\left(J(\theta)\dot{\theta}\right)/\partial\theta$. Thus, the proof is completed. Equation (7) can be further written as

$$\begin{aligned} &\ddot{\boldsymbol{e}}\left(\theta,\dot{\theta},\boldsymbol{l},t\right) \\ &= \begin{bmatrix} H_2(\theta)(\boldsymbol{l}\otimes I) \\ H_1(\theta)\left(\dot{\theta}\otimes I\right) \end{bmatrix}\dot{\theta} + \begin{bmatrix} I \\ J(\theta) \end{bmatrix}\ddot{\theta} + \begin{bmatrix} J^{\mathrm{T}}(\theta) \\ \boldsymbol{0} \end{bmatrix}\dot{\boldsymbol{l}} + \begin{bmatrix} \dot{\boldsymbol{c}} \\ -\ddot{\boldsymbol{r}} \end{bmatrix} \\ &= \begin{bmatrix} H_2(\theta)(\boldsymbol{l}\otimes I) & \boldsymbol{0} \\ H_1(\theta)\left(\dot{\theta}\otimes I\right) & \boldsymbol{0} \end{bmatrix}\begin{bmatrix} \dot{\theta} \\ \boldsymbol{l} \end{bmatrix} + \begin{bmatrix} I & J^{\mathrm{T}}(\theta) \\ J(\theta) & \boldsymbol{0} \end{bmatrix}\begin{bmatrix} \ddot{\theta} \\ \dot{\boldsymbol{l}} \end{bmatrix} + \begin{bmatrix} \dot{\boldsymbol{c}} \\ -\ddot{\boldsymbol{r}} \end{bmatrix}. \end{aligned} \tag{8}$$

Combined Equations (5), (6) and (8), the solution of RMP (3) is converted to obtain the solution of the specific ZND (SZND) model, which is formulated as

$$\dot{\mathbf{y}} = -\left(\lambda I + P^{-1}M\right)\mathbf{y} - P^{-1}(\lambda Q + N) \tag{9}$$

where $\mathbf{y} = \begin{bmatrix} \dot{\theta} \\ \boldsymbol{l} \end{bmatrix}$, $P = \begin{bmatrix} I & J^{\mathrm{T}}(\theta) \\ J(\theta) & \boldsymbol{0} \end{bmatrix}$, $Q = \begin{bmatrix} \boldsymbol{c} \\ -\dot{\boldsymbol{r}} \end{bmatrix}$, $M = \begin{bmatrix} H_2(\theta)(\boldsymbol{l}\otimes I) & \boldsymbol{0} \\ H_1(\theta)\left(\dot{\theta}\otimes I\right) & \boldsymbol{0} \end{bmatrix}$ and $N = \begin{bmatrix} \dot{\boldsymbol{c}} \\ -\ddot{\boldsymbol{r}} \end{bmatrix}$.

Remark 1. It is necessary to illustrate unanimous discretisation both for the classical ZND (6) and the subitem Jacobian, which are not easy to be obtained. Derivative information of the Jacobian matrix with ZND (6) is usually calculated by the MATLAB platform directly. For the situation of an unknown Jacobian matrix, the classical ZND method with two discretisation formulas was presented in [23, 24], in which a backward formula is approximated to estimate the derivative information of the unknown Jacobian matrix. Few literatures emphasize the unanimous discretisation formula in the existing ZND models, which may lead to lower convergent precision of the dynamic system to some extent. Therefore, based on the ZND model (6), we rigorously derive the CTRMP (4) and further develop the specific ZND (SZND) model (9), whose sub-Jacobian matrix can be discretised using the same discrete formula as that of the ZND model.

Remark 2. It is noted that the DRMP (3) is composed of the kinematic energy term. The kinematic energy is an added function of both joint velocities and joint positions. By minimizing kinematic term in (3), we aim to specify a solution that is kinematically feasible and optimal in terms of trajectory and energy efficiency, which is widely applicable in many robotic engineering fields. For the computational complexity per update for the TS-DSZND(14), it contains $(n+m)^3 + 2(m+n)^2 + (7m+9n)$ additions and $(n+m)^3 + 2(m+n)^2 + (5m+9n)$ multipliers. The inverse operator P^{-1} is $(n+m)^3$. Therefore, as m = 3 represents the spatial dimension, the time complexity of (14) is deemed as $O\left(n^3\right)$.

3 | TS-DSZND Model and Theoretical Analyses

For solving the discrete RMP (3), the corresponding SZND model (9) is assumed to be discretised. The general three-step ZeaD formula is presented.

$$\begin{aligned} \dot{\varphi}_k = &\frac{2a}{(3a-1)g}\varphi_{k+1} - \frac{3a+3}{2(3a-1)g}\varphi_k \\ &+ \frac{2}{(3a-1)g}\varphi_{k-1} + \frac{-1-a}{2(3a-1)g}\varphi_{k-2} - \frac{a+1}{3(3a-1)}O(g^2) \end{aligned} \tag{10}$$

with the parameter $a > 1/3$ or $a < -1$. Due to the inconvenience of analysing model stability through Parameter a, we perform a linear transformation $a = 1/(b-1)$ for Equation (10) with $b \in (0,4)$. Then, the following homogenous ZeaD formula is obtained:

$$\begin{aligned}\dot{\varphi}_k = &\frac{2}{(4-b)g}\varphi_{k+1} - \frac{3b}{2(4-b)g}\varphi_k \\ &+ \frac{2(b-1)}{(4-b)g}\varphi_{k-1} - \frac{b}{2(4-b)g}\varphi_{k-2} - \frac{b}{3(4-b)}O(g^2).\end{aligned} \tag{11}$$

Then, applying the above ZeaD Formula (11) to discretise the SZND (9), the following equation is obtained

$$\mathbf{y}_{k+1} \doteq \frac{4-b}{2}g\tilde{\mathbf{y}}_k + \frac{3}{4}b\mathbf{y}_k + (1-b)\mathbf{y}_{k-1} + \frac{1}{4}b\mathbf{y}_{k-2} \tag{12}$$

where $\doteq$ denotes the computational assignment operation. $\tilde{\mathbf{y}}_k = -(\lambda I + P_k^{-1}M_k)\mathbf{y}_k - P_k^{-1}(\lambda Q_k + N_k)$ is defined. As P_k^{-1} and M_k contain θ_k, θ_{k+1} can be computed by the same ZeaD formula (Formula 11):

$$\theta_{k+1} \doteq \frac{4-b}{2}g\dot{\theta}_k + \frac{3}{4}b\theta_k + (1-b)\theta_{k-1} + \frac{1}{4}b\theta_{k-2}. \tag{13}$$

Combining Equation (12) with Equation (13), the following general TS-DSZND model is formulated:

$$\begin{aligned}\begin{bmatrix}\mathbf{y}_{k+1}\\ \theta_{k+1}\end{bmatrix} \doteq &\frac{4-b}{2}g\begin{bmatrix}\tilde{\mathbf{y}}_k\\ \dot{\theta}_k\end{bmatrix} + \frac{3}{4}b\begin{bmatrix}\mathbf{y}_k\\ \theta_k\end{bmatrix} \\ &+ (1-b)\begin{bmatrix}\mathbf{y}_{k-1}\\ \theta_{k-1}\end{bmatrix} + \frac{1}{4}b\begin{bmatrix}\mathbf{y}_{k-2}\\ \theta_{k-2}\end{bmatrix}.\end{aligned} \tag{14}$$

Thus, the resultant three-step discrete SZND (TS-DSZND) model (14) is urgent to be proved zero-stable, consistent and convergence. It is necessary to mention that the convergent constant $\frac{1}{6}b$ is the truncation error constant, which is closely related to the convergence. Besides, P_k^{-1} denotes the inverse matrix of P_k at time instant $t = kg$. Let us focus on the TS-SZND model (14). In particular, $\mathbf{y}_{k+1}, \theta_{k+1}$ is computed using the information available at the previous instant t_k, thereby allowing the DRMP (3) to be carried out during $[t_k, t_{k+1})$. Furthermore, the three initial state vectors $\mathbf{y}_k, \theta_k$ with $k = 0, 1, 2$ are necessary to be set up in the proposed TS-SZND model (14). The first value term $\mathbf{y}_0, \theta_0$ is relative randomly set, and other value terms can be generated by the Euler forward formula [28] to discretise the SZND model (9).

The ith neuron's dynamics (with $i = 1, 2, \ldots n$ and y_{k+1}^i representing the ith entrance of y_k at time instant $t_k = kg$) can be rewritten as

$$\begin{aligned}\mathbf{y}_{k+1}^i = &\frac{3}{4}b\mathbf{y}_k^i + (1-b)\mathbf{y}_{k-1}^i + \frac{1}{4}b\mathbf{y}_{k-2}^i \\ &- \frac{4-b}{2}g\left(\sum_{j=1}^{m+n} w_{ij}\mathbf{y}_k^j - \sum_{j=1}^{m+n} s_j\right)\end{aligned} \tag{15}$$

where w_{ij} and s_{ij} represent the corresponding elements of matrices $-\lambda I + P_k^{-1}M_k$ and $\lambda P_k^{-1}Q_k + P_k^{-1}N_k$, respectively. The specific structure of the TS-DSZND (14) is displayed in Figure 1 for solving the DRMP (3) to facilitate hardware realization. It is facilitated for the fast execution of digital computers with plant-scale iterations.

Theorem 2. *The general TS-DSZND model (14) is zero-stable and consistent, which converges with the truncation error order $O(g^3)$, when $b \in (0,4)$. As b tends to 0, better accuracy of the TS-DSZND (4) is acquired.*

Proof: Zero stability is the property when the stepsize $g \to 0$ is satisfied. The characteristic polynomial of the differential equation (Equation 14) is expressed as follows:

$$\begin{aligned}\psi(\eta) &= 2\eta^3 - \frac{3b}{2}\eta^2 + 2(b-1)\eta - \frac{b}{2} \\ &= (\eta-1)\left(2\eta^2 + \left(2 - \frac{3b}{2}\right)\eta + \frac{b}{2}\right)\end{aligned} \tag{16}$$

which has one root $\eta_1 = 1$. Under the condition of $b \in (0,4)$, the other roots satisfy $|\eta_{2,3}| < 1$. Thus, according to Result 1 in Appendix, the TS-DSZND (14) is zero-stable. Besides, it yields

$$\begin{aligned}\begin{bmatrix}\mathbf{y}_{k+1}\\ \theta_{k+1}\end{bmatrix} = &\frac{4-b}{2}g\begin{bmatrix}\tilde{\mathbf{y}}_k\\ \dot{\theta}_k\end{bmatrix} + \frac{3}{4}b\begin{bmatrix}\mathbf{y}_k\\ \theta_k\end{bmatrix} \\ &+ (1-b)\begin{bmatrix}\mathbf{y}_{k-1}\\ \theta_{k-1}\end{bmatrix} + \frac{1}{4}b\begin{bmatrix}\mathbf{y}_{k-2}\\ \theta_{k-2}\end{bmatrix} + \frac{1}{6}bO(g^3).\end{aligned} \tag{17}$$

According to Result 2, it is consistent with truncation order $O(g^3)$. Therefore, according to Result 3, the zero stability and consistence leads to the convergence of (14). The TS-DSZND model (14) converges with the order of truncation error being

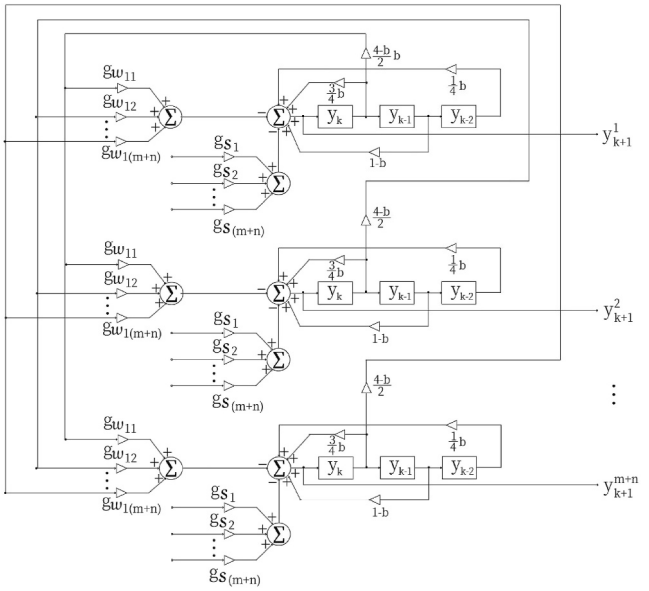


FIGURE 1 | Neuron structure of the TZ-DSZND model (14) for solving DRMP (3).

$O(g^3)$. Obviously, as b tends to 0, the term of $bO(g^3)$ results in 0. The proof is completed.

Theorem 3. *With a specific time step g of the TS-DSZND model (14) satisfying* $g \in (0, 1)$*, the effective stability domain of* $\mu = \lambda g$ *is* $\left(0, \min\left\{4b/(4-b), (16+b^2-8b)/(-b^2+4b)\right\}\right)$ *and the optimal parameter for the effective stability domain b is* 4/3.

Proof: Discretising ZND Formula (6) directly using ZeaD Formula (11), we obtain

$$\mathbf{e}_{k+1} = \left(\frac{b-4}{2}\mu + \frac{3}{4}b\right)\mathbf{e}_k + (1-b)\mathbf{e}_{k-1} + \frac{1}{4}b\mathbf{e}_{k-2} \tag{18}$$

where $\mu = \lambda g$. The characteristic polynomial of Equation (18) can be expressed as

$$\psi(\widehat{\eta}) = \widehat{\eta}^3 - \left(\frac{b-4}{2}\mu + \frac{3}{4}b\right)\widehat{\eta}^2 + (b-1)\widehat{\eta} - \frac{1}{4}b. \tag{19}$$

According to the Jury criterion in [29], all three roots of $\psi(\widehat{\eta}) = 0$ are less than 1 (i.e., $|\widehat{\eta}_i| < 1, i = 1, 2, 3.$) satisfying

$$\begin{cases} 0 < b < 4, \\ \mu < \dfrac{16 + b^2 - 8b}{-b^2 + 4b}, \\ \mu < \dfrac{4b}{4-b}. \end{cases} \tag{20}$$

For illustrating the relationship between b and μ intuitively, the relationship between Parameter b and Parameter μ is shown in Figure 2. As can be seen from Figure 2, the maximum stability domain μ can reach 2, whereas the value of b equals 4/3. Thus, the proof is completed. Besides, the effective stability domain of the TS-DSZND model (14) with various values b is displayed in Table 2.

4 | Numerical Verifications

Upon the above discussions, various path-tracking experiments are conducted to verify the superiority and effectiveness of the proposed TS-DSZND model (14) as well as the effective stability domain. For comparisons, Euler discretisation is also adopted for solving the SZND (9). The following Euler-discretised SZND (E-DSZND) model is presented in [28].

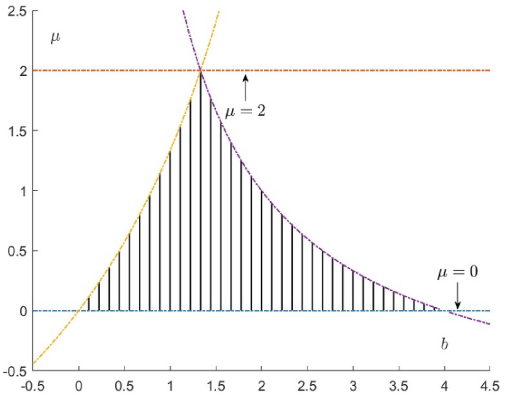


FIGURE 2 | Effective domain of TS-DSZND (14) with the parameters $\mu = \lambda g$ and b.

$$\begin{bmatrix} \mathbf{y}_{k+1} \\ \theta_{k+1} \end{bmatrix} \doteq g\begin{bmatrix} \tilde{\mathbf{y}}_k \\ \dot{\theta}_k \end{bmatrix} + \begin{bmatrix} \mathbf{y}_k \\ \theta_k \end{bmatrix} \tag{21}$$

where $\tilde{\mathbf{y}}_k = -\left(\lambda I + P_k^{-1}M_k\right)\mathbf{y}_k - P_k^{-1}(\lambda Q_k + N_k)$. And it is worth mentioning that E-DSZND (21) has a $O(g^2)$ pattern, and its stepsize domain is (0,2).

4.1 | Path Tracking With Three-Link Planar Manipulators

Firstly, a planar manipulator of three rotatable links is studied. The manipulator is assigned to track a hypocycloid path, which is expressed as

$$\mathbf{r_k} = \begin{bmatrix} 2 + 0.08\cos(4t_k) + 0.32\cos(t_k) \\ 0.5 - 0.08\sin(4t_k) + 0.32\sin(t_k) \end{bmatrix}.$$

It is obvious that for TS-DSZND (14), three initial vectors (i.e., $\mathbf{y}_0, \mathbf{y}_1, \mathbf{y}_2$) are demanded to be set. Then, θ_0 is randomly chosen as $\theta_0 = [1.095, -1.154, -0.277]^{\mathrm{T}}(\mathrm{rad})$ and $\mathbf{y}_0 = [0, 0, 0, 0, 0]^{\mathrm{T}}$. Meanwhile, $\mathbf{y}_1$ and $\mathbf{y}_2$ can be generated by the Euler discrete formula. We define a residual error $\|\mathbf{e}_{k+1}\|_2 = \left\|\left[\dot{\theta}_{k+1} + \boldsymbol{c}_{k+1} + J^{\mathrm{T}}(\theta_{k+1})\boldsymbol{l}_{k+1}, J(\theta_{k+1})\dot{\theta}_{k+1} - \dot{\boldsymbol{r}}_{k+1}\right]^{\mathrm{T}}\right\|_2$ at time instant t_k with time step $g = 0.01$ s. The task duration is $t_{\mathrm{f}} = 20$ s, where $\mathbf{y}_{k+1} = \left[\dot{\theta}_{k+1}, \boldsymbol{l}\right]^{\mathrm{T}}$.

The corresponding simulated results generated by the TS-DSZND model (14) are presented in Figure 3. From Figure 3a and b, we can observe that the manipulator completes the tracking task smoothly. The trajectory of the end effector matches well with the desired trajectory in dotted lines. Besides, $\theta_{k+1} = \left[\theta_{k+1,1}, \theta_{k+1,2}, \theta_{k+1,3}\right]^{\mathrm{T}}$ are depicted in Figure 3c. The residual error synthesised by the TS-DSZND model (14) with a different parameter, b, in Table 2 and the E-DSZND model (21) are presented in Figure 3d–f together. A different stepsized domain, $\mu = \lambda g$, is set. Obviously, the traditional E-DSZND model (21) can remain convergent in all three case,s but it is not as good as the TS-DSZND model in terms of convergent accuracy. In Figure 3d, the residual error of five TS-DSZND models listed in Table 2 is around 10^{-5} in the end. And the smaller the parameter b is applied, the better performance in convergence accuracy is obtained, which is fully illustrated in Figure 3d. These observations well substantiate the validity of Theorem 2. Moreover in Figure 3e, as the stepsize μ increases to 0.5, the residual error of the TS-DSZND-1 model and the TS-DSZND-5 model fail to converge, whereas the other three models remain with high convergent precision. At the same time, as we continue to increase the stepsize μ to 1, only TS-DSZND-3 remains stable, which is shown in Figure 3f. These experimental results respond to the theoretical results in Theorem 3.

TABLE 2 | Formulations and comparisons of different TS-DSZND models (14) with various parameters.

Parameter b	TS-DSZND model	Effective stepsize domain μ	Truncation error	Label
$\frac{1}{5}$	$\begin{bmatrix} \mathbf{y}_{k+1} \\ \theta_{k+1} \end{bmatrix} \doteq \frac{19}{10} g \begin{bmatrix} \tilde{\mathbf{y}}_k \\ \dot{\theta}_k \end{bmatrix} + \frac{3}{20} \begin{bmatrix} \mathbf{y}_k \\ \theta_k \end{bmatrix} + \frac{4}{5} \begin{bmatrix} \mathbf{y}_{k-1} \\ \theta_{k-1} \end{bmatrix} + \frac{1}{20} \begin{bmatrix} \mathbf{y}_{k-2} \\ \theta_{k-2} \end{bmatrix}$	$\left(0, \frac{4}{19}\right)$	$\frac{1}{30} O(g^3)$	TS-DSZND-1
$\frac{1}{2}$	$\begin{bmatrix} \mathbf{y}_{k+1} \\ \theta_{k+1} \end{bmatrix} \doteq \frac{7}{4} g \begin{bmatrix} \tilde{\mathbf{y}}_k \\ \dot{\theta}_k \end{bmatrix} + \frac{3}{4} \begin{bmatrix} \mathbf{y}_k \\ \theta_k \end{bmatrix} + \frac{1}{2} \begin{bmatrix} \mathbf{y}_{k-1} \\ \theta_{k-1} \end{bmatrix} + \frac{1}{8} \begin{bmatrix} \mathbf{y}_{k-2} \\ \theta_{k-2} \end{bmatrix}$	$\left(0, \frac{4}{7}\right)$	$\frac{1}{12} O(g^3)$	TS-DSZND-2
$\frac{4}{3}$	$\begin{bmatrix} \mathbf{y}_{k+1} \\ \theta_{k+1} \end{bmatrix} \doteq \frac{8}{3} g \begin{bmatrix} \tilde{\mathbf{y}}_k \\ \dot{\theta}_k \end{bmatrix} + \begin{bmatrix} \mathbf{y}_k \\ \theta_k \end{bmatrix} - \frac{1}{3} \begin{bmatrix} \mathbf{y}_{k-1} \\ \theta_{k-1} \end{bmatrix} + \frac{1}{3} \begin{bmatrix} \mathbf{y}_{k-2} \\ \theta_{k-2} \end{bmatrix}$	(0,2)	$\frac{2}{9} O(g^3)$	TS-DSZND-3
2	$\begin{bmatrix} \mathbf{y}_{k+1} \\ \theta_{k+1} \end{bmatrix} \doteq g \begin{bmatrix} \tilde{\mathbf{y}}_k \\ \dot{\theta}_k \end{bmatrix} + \frac{3}{2} \begin{bmatrix} \mathbf{y}_k \\ \theta_k \end{bmatrix} - \begin{bmatrix} \mathbf{y}_{k-1} \\ \theta_{k-1} \end{bmatrix} + \frac{1}{2} \begin{bmatrix} \mathbf{y}_{k-2} \\ \theta_{k-2} \end{bmatrix}$	(0,1)	$\frac{1}{3} O(g^3)$	TS-DSZND-4
3	$\begin{bmatrix} \mathbf{y}_{k+1} \\ \theta_{k+1} \end{bmatrix} \doteq \frac{1}{2} g \begin{bmatrix} \tilde{\mathbf{y}}_k \\ \dot{\theta}_k \end{bmatrix} + \frac{9}{4} \begin{bmatrix} \mathbf{y}_k \\ \theta_k \end{bmatrix} - 2 \begin{bmatrix} \mathbf{y}_{k-1} \\ \theta_{k-1} \end{bmatrix} + \frac{3}{4} \begin{bmatrix} \mathbf{y}_{k-2} \\ \theta_{k-2} \end{bmatrix}$	$\left(0, \frac{1}{3}\right)$	$\frac{1}{2} O(g^3)$	TS-DSZND-5

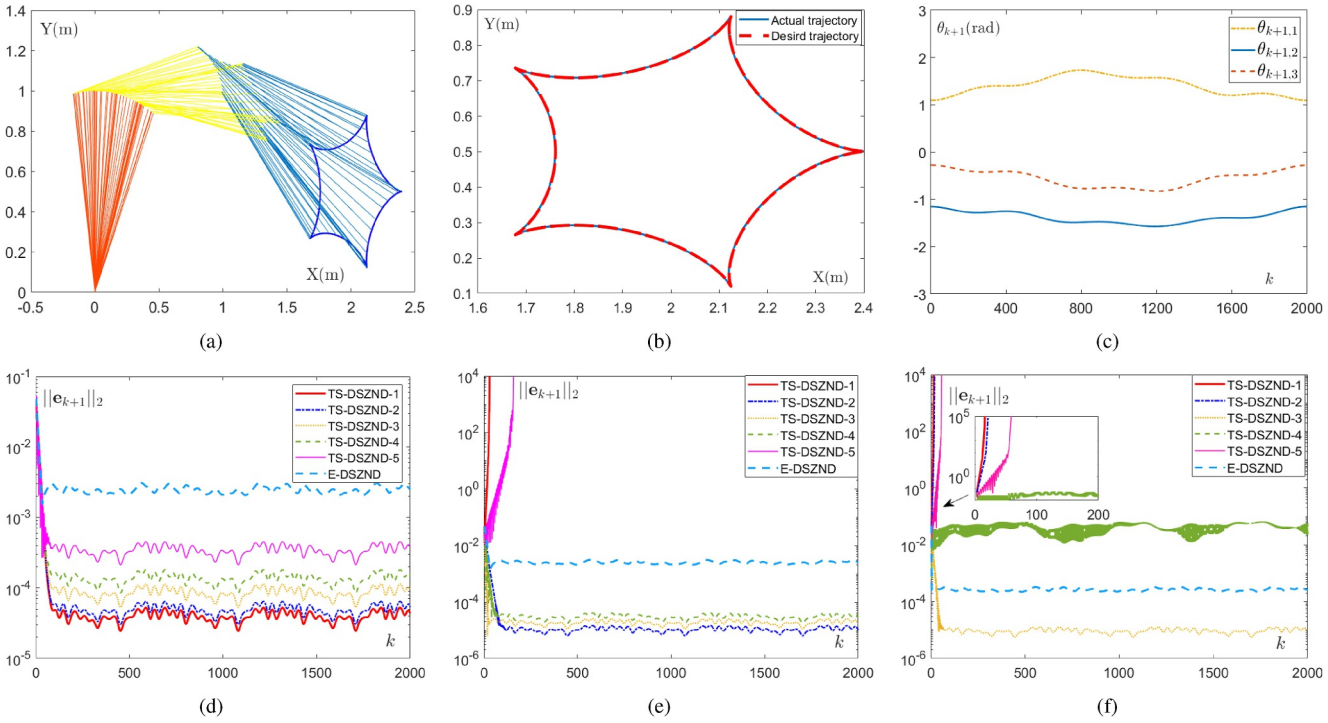


FIGURE 3 | Trajectory profiles of the manipulator, end effector, joint angles $\theta_{k+1} = [\theta_{k+1,1}, \theta_{k+1,2}, \theta_{k+1,3}]$ and tracking error synthesized by TS-DSZND models (14) in Table 2 E-DSZND (21) with $g = 0.01$ s. (a) Manipulator trajectories synthesized by TS-DSZND-1 with $\mu = 0.1$. (b) Actual trajectory and desired trajectory. (c) Joint angle profiles. (d) Tracking error with Stepsize $\mu = 0.1$. (e) Tracking error with Stepsize $\mu = 0.5$. (f) Tracking error with Stepsize $\mu = 1$.

4.2 | Path Tracking With PA10

As another example, the consultant PA10 manipulator is expected to execute a flower path, which is expressed as

$$\mathbf{r_k} = \begin{bmatrix} 0.2 + 0.2\cos(2t_k)\cos(t_k) \\ 0.2 + 0.2\cos(2t_k)\sin(t_k) \\ 0.6 + 0.25\cos^2(2t_k) \end{bmatrix}.$$

The seven initial joint states are set as $\theta_0 = [0.532, 0.903, 0.081, -0.727, 0.002, -0.125, 0]^{\mathrm{T}}$(rad) and the initial states of $\mathbf{y}(0)$ are set as $\mathbf{y}_0 = [0.197, -0.077, -0.181, 0.289, -0.005, 0.054, 0, -0.427, -0.710]^{\mathrm{T}}$. Besides, we set the time step as $g = 0.001$ s, and task duration $t_{\mathrm{f}} = 20$ s is introduced. The residual error is defined as the same in Section 4.1. The kinematic realization of the PA10 manipulator is presented in Figure 4. As depicted in Figure 4a and b, we can see that the PA10 manipulator successfully completes the flower task and the trajectory of the

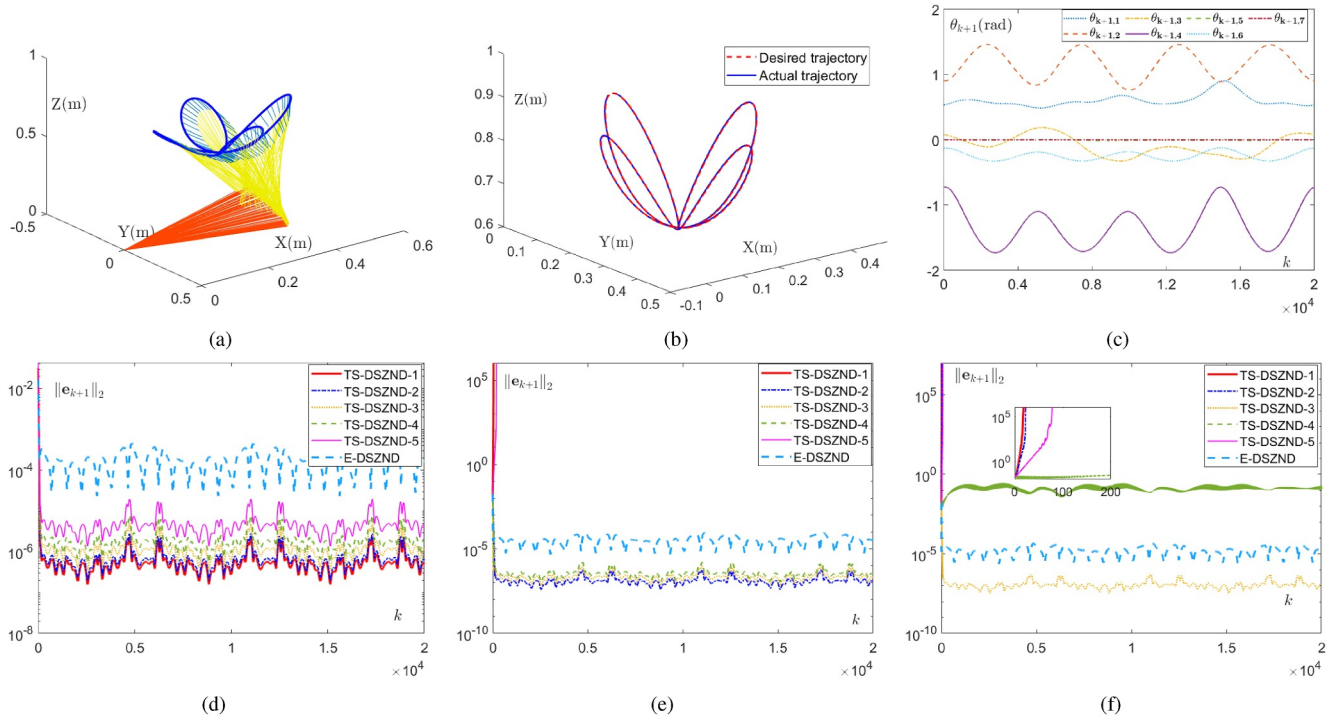


FIGURE 4 | Trajectory profiles of the TS-DSZND models in Table 2 and E-DSZND (21) with $g = 0.001$ s. (a) Manipulator trajectories. (b) Actual trajectory and desired trajectory. (c) Kinematic joint angles. (d) Tracking error with $\mu = 0.1$. (e) Tracking error with $\mu = 0.5$. (f) Tracking error with $\mu = 1$.

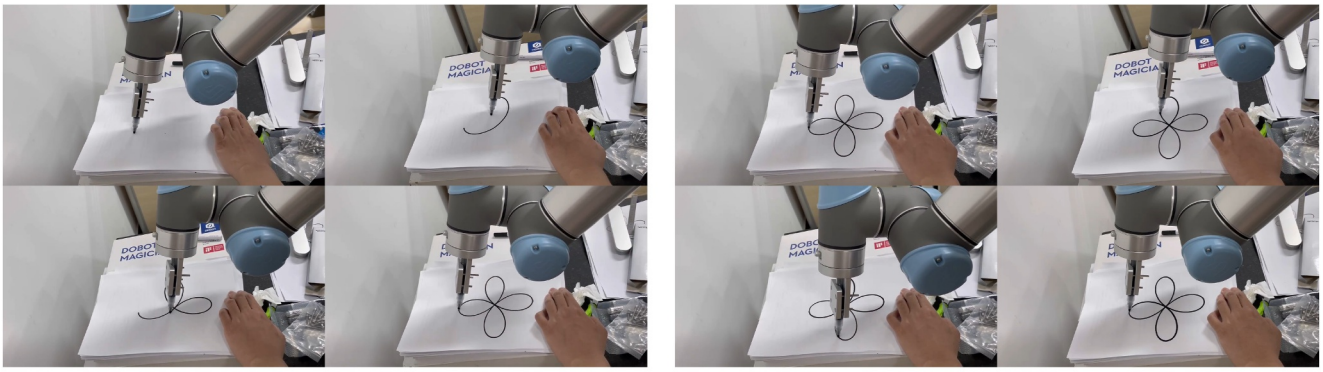


FIGURE 5 | Tracking profiles synthesised by the TS-DSZND-3 model (14) for chasing a four-leaved clover curve with UR5 manipulator. (a) Snapshots of the end-effector with first tracking cycle. (b) Snapshots of the end-effector with second cycle.

end effector overlaps with the desired trajectory. Besides, the state profiles of the seven joint angles $\theta_{k+1} = [\theta_{k+1,1}, \theta_{k+1,2}, \theta_{k+1,3}, \theta_{k+1,4}, \theta_{k+1,5}, \theta_{k+1,6}, \theta_{k+1,7}]^{\mathrm{T}}$ are visualized in Figure 4c. And the residual errors of different models with different stepsizes denoted by μ are displayed in Figure 4d–f. Similarly, the convergent precision of the TS-DSZND model (14) with a different parameter b (listed in Table 2) is lower than the corresponding E-DSZND model (21) for the DRMP (3). Specially, the residual error synthesized by the different TS-DSZND models (14) (listed in Table 2) with $\mu = 0.1$ reaches to 10^{-6} in the end, which is visualized in Figure 4d. As can be seen in Figure 4e, the TS-DSZND-1 model and TS-DSZND-5 have diverged as μ increases to 0.5. Subsequently in Figure 4f, only the TS-DSZND-3 model and the E-DSZND model keep stable by the stepsize $\mu = 1$. In summary, the proposed TS-DSZND (14) is verified for solution of the DRMP (3).

5 | Physical Verifications Based on the UR5 Manipulator

To illustrate the physical capability of the proposed TS-DSZND model (14), experiments on real the UR5 manipulator with six DOFs are provided in Figure 5. The UR5 manipulator works in a 3-D space, and the D-H parameter of the UR5 manipulator can be found in Table 3. The kinematic process of the physical experiment can be divided into the following two parts. First, a pen is installed on the end effector of the UR5 manipulator to

TABLE 3 | D-H parameters of the UR5 manipulator.

Joint	θ_i (rad)	a_i (m)	d_i (m)	α_i (rad)
1	θ_1	0	0.089159	$\pi/2$
2	θ_2	-0.425	0	0
3	θ_3	-0.39225	0	0
4	θ_4	0	0.10915	$\pi/2$
5	θ_5	0	0.09465	$-\pi/2$
6	θ_6	0	0.0823	0

draw the desired path. Second, a set of movement snapshots of the redundant manipulator UR5 is captured. The time step $g = 0.002$ s and $\mu = \lambda g = 0.5$ are predefined. We apply TS-DSZND-3 to carry out the given task. The task duration $t_f = 12$ s is set and the desired trajectory supposed to trace a four-leaved clover curve, which can be expressed as

$$\mathbf{r_k} = \begin{bmatrix} 0.5 + 0.075\cos(2t_k)\cos(t_k) \\ 0.075\cos(2t_k)\sin(t_k) \\ 0.1088 \end{bmatrix}.$$

In the experiment, the UR5 manipulator driven by the TS-DSZND model (14) executes the given task smoothly and precisely while the orientation of the end effector with the UR5 manipulator is fixed, assuring the validity of the proposed TS-DSZND. The executing procedure snapshots are displayed in Figure 5. We can observe the end effector is tracking a four-leaved clover curve smoothly at a different time instant. Figure 5a depicts the kinematic procedure of the end effector from any arbitrary joint position. At last, all the flexible joints return to their initial states. In Figure 5b, the target manipulator continues to move along the desired trajectory successfully, indicating perfective fitting of the DRMP scheme (3) via the proposed TS-DSZND (14) in real application.

6 | Conclusion

For well strengthening the discrete model for kinematic control of redundant manipulators with accurate Jacobian matrix estimation, an SZND model (9) is constructed in this paper. Then, by applying a three-step ZeaD formula (Formula 11), the TS-DSZND model (14) with a precise Jacobian matrix is proposed. Theoretical analyses ensure the efficiency of the proposed TS-DSZND model (14) for precise tracking of the manipulators. Simulative examples on different manipulators (i.e., three-link manipulator, PA10 manipulator and UR5 manipulator) verified the effectiveness and better performance of the TS-DSZND model. A future work may lie on the direction of a general multistep method with a ZNN model for solving the cooperation of multiple manipulators.

Acknowledgements

This work was supported by National Natural Science Foundation of China (Grant No. U22A20102), Natural Science Foundation of Zhejiang Province (Grant No. LZY22E050002), Scientific Research Project funded by Zhejiang Provincial Department of Education (Y202455182) and "Pioneer" and "Leading Goose" R&D Program of Zhejiang Province (Grant No. 2023C01150).

Conflicts of Interest

The authors declare no conflicts of interest.

Data Availability Statement

The data that support the findings of this study are available from the corresponding author upon reasonable request.

References

1. J. Fan, L. Jin, P. Li, J. Liu, Z.-G. Wu, and W. Chen, "Coevolutionary Neural Dynamics Considering Multiple Strategies for Nonconvex Optimization," *Tsinghua Science and Technology* (2025), https://doi.org/10.26599/TST.2025.901012.

2. M. Liu, L. Chen, X. Du, L. Jin, and M. Shang, "Activated Gradients for Deep Neural Networks," *IEEE Transactions on Neural Networks and Learning Systems* 34, no. 4 (2023): 2156–2168, https://doi.org/10.1109/tnnls.2021.3106044.

3. A. Hentout, A. Maoudj, and A. Kouider, "Shortest Path Planning and Efficient Fuzzy Logic Control of Mobile Robots in Indoor Static and Dynamic Environments," *Romanian Journal of Information Science and Technology* 27, no. 1 (2024): 21–36, https://doi.org/10.59277/romjist.2024.1.02.

4. Z. Cui, Y. Huang, W. Li, P. W. Y. Chiu, and Z. Li, "Noise-Resistant Adaptive Gain Recurrent Neural Network for Visual Tracking of Redundant Flexible Endoscope Robot With Time-Varying State Variable Constraints," *IEEE Transactions on Industrial Electronics* 71, no. 3 (2024): 2694–2704, https://doi.org/10.1109/tie.2023.3270533.

5. M. Liu, Y. Li, Y. Chen, Y. Qi, and L. Jin, "A Distributed Competitive and Collaborative Coordination for Multirobot Systems," *IEEE Transactions on Mobile Computing* 23, no. 12 (2024): 11436–11448, https://doi.org/10.1109/tmc.2024.3397242.

6. R.-E. Precup, C.-A. Bojan, K. Gao, and S. Cui, "Problem Setting for Trajectory Planning and Cruise Control of a Connected Autonomous Electric Bus in Intersection Scenarios With Human-Driven Vehicles to Optimize Energy, Comfort and Tracking," *Romanian Journal of Information Science and Technology* 28, no. 3 (2025): 299–312, https://doi.org/10.59277/ROMJIST.2025.3.05.

7. B. Liao, L. Han, X. Cao, S. Li, and J. Li, "Double Integral-Enhanced Zeroing Neural Network With Linear Noise Rejection for Time-Varying Matrix Inverse," *CAAI Transactions on Intelligence Technology* 9, no. 1 (2024): 197–210, https://doi.org/10.1049/cit2.12161.

8. W. Song and S. Tong, "Inverse Reinforcement Learning Optimal Control for Takagi-Sugeno Fuzzy Systems," *Artificial Intelligence Science and Engineering* 1, no. 2 (2025): 134–146, https://doi.org/10.23919/aise.2025.000010.

9. H. Huang, L. Jin, and Z. Zeng, "A Momentum Recurrent Neural Network for Sparse Motion Planning of Redundant Manipulators With majorization-minimization," *IEEE Transactions on Industrial Electronics* 72, no. 12 (2025): 13532–13541, https://doi.org/10.1109/TIE.2025.3566731.

10. L. Xiao, S. Li, F.-J. Lin, Z. Tan, and A. H. Khan, "Zeroing Neural Dynamics for Control Design: Comprehensive Analysis on Stability, Robustness, and Convergence Speed," *IEEE Transactions on Industrial Informatics* 15, no. 5 (2019): 2605–2616, https://doi.org/10.1109/tii.2018.2867169.

11. S. Li, J. He, Y. Li, and M. U. Rafique, "Distributed Recurrent Neural Networks for Cooperative Control of Manipulators: A Game-Theoretic Perspective," *IEEE Transactions on Neural Networks and Learning*

Systems 28, no. 2 (2017): 415–426, https://doi.org/10.1109/tnnls.2016.2516565.

12. Z. Li, S. Li, and X. Luo, "An Overview of Calibration Technology of Industrial Robots," *IEEE/CAA Journal of Automatica Sinica* 8, no. 1 (2021): 23–26, https://doi.org/10.1109/jas.2020.1003381.

13. Y. Zhang, L. He, C. Hu, J. Guo, J. Li, and Y. Shi, "General Four-Step Discrete-Time Zeroing and Derivative Dynamics Applied to Time-Varying Nonlinear Optimization," *Journal of Computational and Applied Mathematics* 347 (2019): 314–329, https://doi.org/10.1016/j.cam.2018.08.017.

14. B. Qiu, J. Guo, X. Li, Z. Zhang, and Y. Zhang, "Discrete-Time Advanced Zeroing Neurodynamic Algorithm Applied to Future Equality-Constrained Nonlinear Optimization With Various Noises," *IEEE Transactions on Cybernetics* 52, no. 5 (2022): 3539–3552, https://doi.org/10.1109/tcyb.2020.3009110.

15. H. Zhang, Y. Huang, N. Zhao, and P. Shi, "Improved Event-Triggered Adaptive Neural Network Control for Multi-Agent Systems Under Denial-of-Service Attacks," *Artificial Intelligence in Science and Engineering* 1, no. 2 (2025): 122–133, https://doi.org/10.23919/aise.2025.000009.

16. D. Wang, D. Liu, Q. Zhang, and D. Zhao, "Data-Based Adaptive Critic Designs for Nonlinear Robust Optimal Control With Uncertain Dynamics," *IEEE Transactions on Systems, Man, and Cybernetics: Systems* 46, no. 11 (2016): 1544–1555, https://doi.org/10.1109/tsmc.2015.2492941.

17. W. Yang, S. Li, Z. Li, and X. Luo, "Highly-Accurate Manipulator Calibration via Extended Kalman Filter-Incorporated Residual Neural Network," *IEEE Transactions on Industrial Informatics* 19, no. 11 (2023): 10831–10841, https://doi.org/10.1109/tii.2023.3241614.

18. Y. Zhang, D. Jiang, and J. Wang, "A Recurrent Neural Network for Solving Sylvester Equation With Time-Varying Coefficients," *IEEE Transactions on Neural Networks* 13, no. 5 (2002): 1053–1063, https://doi.org/10.1109/tnn.2002.1031938.

19. L. Jin, Z. Su, D. Fu, and X. Xiao, "Coevolutionary Neural Solution for Nonconvex Optimization With Noise Tolerance," *IEEE Transactions on Neural Networks and Learning Systems* 35, no. 12 (2024): 17571–17582, https://doi.org/10.1109/tnnls.2023.3306374.

20. Y. Zhang, Y. Ling, M. Yang, S. Yang, and Z. Zhang, "Inverse-Free Discrete ZNN Models Solving for Future Matrix Pseudoinverse via Combination of Extrapolation and Zead Formulas," *IEEE Transactions on Neural Networks and Learning Systems* 32, no. 6 (2021): 2663–2675, https://doi.org/10.1109/tnnls.2020.3007509.

21. B. Liao, Y. Zhang, and L. Jin, "Taylor O(h3) Discretization of ZNN Models for Dynamic Equality-Constrained Quadratic Programming With Application to Manipulators," *IEEE Transactions on Neural Networks and Learning Systems* 27, no. 2 (2016): 225–238, https://doi.org/10.1109/TNNLS.2015.2435014.

22. Y. Kong, Y. Jiang, and X. Xia, "Terminal Recurrent Neural Networks for Time-Varying Reciprocal Solving With Application to Trajectory Planning of Redundant Manipulation," *IEEE Transactions on Systems, Man, and Cybernetics: Systems* 52, no. 1 (2022): 387–399, https://doi.org/10.1109/tsmc.2020.2998485.

23. Y. Zhang, H. Gong, M. Yang, J. Li, and X. Yang, "Stepsize Range and Optimal Value for Taylorzhang Discretization Formula Applied to Zeroing Neurodynamics Illustrated via Future Equality-Constrained Quadratic Programming," *IEEE Transactions on Neural Networks and Learning Systems* 30, no. 3 (2019): 959–967, https://doi.org/10.1109/tnnls.2018.2861404.

24. J. Li, Y. Zhang, and M. Mao, "General Square-Pattern Discretization Formulas via Second-Order Derivative Elimination for Zeroing Neural Network Illustrated by Future Optimization," *IEEE Transactions on Neural Networks and Learning Systems* 30, no. 3 (2019): 891–901, https://doi.org/10.1109/tnnls.2018.2853732.

25. M. Yang, Y. Zhang, H. Hu, and B. Qiu, "General 7-Instant DCZNN Model Solving Future different-level System of Nonlinear Inequality and Linear Equation," *IEEE Transactions on Neural Networks and Learning Systems* 31, no. 9 (2020): 3204–3214, https://doi.org/10.1109/tnnls.2019.2938866.

26. J. Li, Y. Zhang, S. Li, and M. Mao, "New Discretization-Formulabased Zeroing Dynamics for Real-Time Tracking Control of Serial and Parallel Manipulators," *IEEE Transactions on Industrial Informatics* 14, no. 8 (2018): 3416–3425, https://doi.org/10.1109/tii.2017.2780892.

27. Z. Zhang, S. Chen, and J. Liang, "Discrete-Time Circadian Rhythms Neural Network for Perturbed Redundant Robot Manipulators Tracking Problem With Periodic Noises," *IEEE Transactions on Industrial Informatics* 18, no. 1 (2022): 242–251, https://doi.org/10.1109/tii.2021.3065715.

28. Y. Zhang, S. Chen, S. Li, and Z. Zhang, "Adaptive Projection Neural Network for Kinematic Control of Redundant Manipulators With Unknown Physical Parameters," *IEEE Transactions on Industrial Electronics* 65, no. 6 (2018): 4909–4920, https://doi.org/10.1109/tie.2017.2774720.

29. E. I. Jury, "A Note on the Modified Stability Table for Linear Discrete Time Systems," *IEEE Transactions on Circuits and Systems* 38, no. 2 (1991): 221–223, https://doi.org/10.1109/31.68301.

30. J. D. Lambert, *Numerical Methods for Ordinary Differential Systems: The Initial Value Problem* (Wiley, 1991).

Appendix A

The following results from [30] are presented for the basis of theoretical analyses. Given a general linear k-step rule $\sum_{j=0}^{k}\alpha_j y_{i+j} = h\sum_{j=0}^{k}\beta_j f_{i+j}$. The zero stability of a linear k-step method can be studied by its following characteristic polynomial: $\rho(\xi) = \sum_{i=0}^{k}\alpha_i \xi^i$.

Result 1. *The linear k-step method is said to be zero-stable if no root of the characteristic polynomial $\rho(\xi)$ has a modulus greater than one and if every root with modulus one is simple.*

Result 2. *The linear k-step method is said to be consistent of Order p if the truncation error for the exact solution is of Order $O(h^{p+1})$ where $p > 0$.*

Result 3. *The linear k-step method is convergent with the order of its truncation error, if and only if the method is zero-stable and consistent.*